Research Article Vol. 13, No. 9 / September 2026 / Optica 1735

OPTICA

Twist-controlled Goos–Hänchen shift and electron–hole asymmetry in bilayer graphene

Jiaxing Tu,[1,†] Xiaofeng Li,[1,2,3,†] Yunpeng Yan,[1] Xiao Li,[2,9] Xinxing Zhou,[4,5,10] Hui Jing,[4,6] Leman Kuang,[4,6] Xianfeng Chen,[7] Jianguo Tian,[1] and Zhibo Liu[1,8,*]

[1]The Key Laboratory of Weak Light Nonlinear Photonics, Ministry of Education, School of Physics and Teda Applied Physics Institute, State Key Laboratory of Photovoltaic Materials and Cells, Nankai University, Tianjin 300071, China
[2]Department of Physics, City University of Hong Kong, Kowloon, Hong Kong SAR 999077, China
[3]School of Physics, Electronics and Intelligent Manufacturing, Huaihua University, Huaihua 418000, China
[4]Key Laboratory of Low-Dimensional Quantum Structures and Quantum Control of Ministry of Education, School of Physics and Electronics, Hunan Normal University, Changsha 410081, China
[5]Key Laboratory of Physics and Devices in Post-Moore Era, College of Hunan Province, Changsha 410081, China
[6]Academy for Quantum Science and Technology, Zhengzhou University of Light Industry, Zhengzhou 450002, China
[7]State Key Laboratory of Advanced Optical Communication Systems and Networks, School of Physics and Astronomy, Shanghai Jiao Tong University, Shanghai 200240, China
[8]The Collaborative Innovation Center of Extreme Optics, Shanxi University, Taiyuan 030006, China
[9]xiao.li@cityu.edu.hk
[10]xinxingzhou@hunnu.edu.cn
[†]These authors contributed equally to this work.
*zbliu@nankai.edu.cn

Received 9 April 2026; revised 1 July 2026; accepted 25 July 2026; published 31 August 2026

Twisted bilayer graphene (TBG) provides a versatile platform for quantum state engineering, yet its high-energy electron–hole asymmetry remains experimentally elusive due to optical broadening in traditional absorption spectra. Here, we demonstrate the precise control of the Goos–Hänchen (GH) shift in TBG by manipulating the interlayer twist angle. By leveraging the GH shift's intrinsic sensitivity to phase gradients, we report what we believe is the first experimental observation of the predicted splitting in the complex refractive index ($\tilde{n}$) at van Hove singularities for large twist angles ($\theta > 10°$). Our measurements reveal a splitting interval below 100 meV, which is associated with the interlayer distance and interlayer coupling of TBG. These findings establish GH shift spectroscopy as a powerful phase-sensitive probe for moiré superlattices, surpassing conventional optical methods in resolving fine band-structure features and informing the design of moiré-based optoelectronics.

https://doi.org/10.1364/OPTICA.601328

1. INTRODUCTION

Twisted bilayer graphene (TBG) has emerged as a paradigmatic platform for quantum state engineering via its tunable moiré superlattice [1–5]. The interlayer twist angle serves as a powerful knob, dramatically reconstructing the electronic band structure and giving rise to remarkable phenomena including van Hove singularities (VHSs) [6–10], correlated insulating states [11,12], and unconventional superconductivity [13]. Of particular significance is the theoretically predicted splitting of the complex refractive index ($\tilde{n}$) in large-angle regimes ($\theta > 10°$), originating from electron–hole asymmetry near VHSs energies [7,14–16]. This high-energy regime complements rather than competes with the low-energy "magic-angle" physics: while the latter features correlated states near the Fermi level [1–4], the former provides access to interlayer coupling asymmetries and optical resonances that are essential for understanding moiré-induced dielectric responses and optoelectronic functionality [14,15]. However, this critical signature has remained experimentally elusive due to the inherent limitations of conventional optical techniques, such as absorption spectroscopy, which suffer from substantial optical broadening effects [7,17]. This challenge underscores the need for novel experimental approaches with enhanced sensitivity to interfacial dielectric modifications.

The Goos–Hänchen (GH) shift—a lateral displacement of reflected light arising from interfacial phase gradients—emerges as an ideal probe for this challenge. While initially characterized in classical optics [18], the GH shift has recently been recognized as a sensitive interferometric tool that encodes phase information about light–matter interactions, providing exceptional resolution of a material's dielectric function [19]. Although GH shifts have been successfully employed to investigate two-dimensional (2D) materials [20–27] and topological systems [28,29], pioneering theoretical studies have already proposed the application of optical beam shifts to moiré systems. Specifically, the photonic spin Hall

effect and Imbert–Fedorov shifts were theoretically predicted to exhibit clear fingerprints of the underlying moiré pattern in bilayer graphene, establishing a direct link between beam displacements and the system's electronic conductivity [30]. Furthermore, subsequent theoretical calculations demonstrated that both spin splitting and GH shifts in twisted bilayer graphene (TBG) are highly twist-angle-dependent [31]. Despite these vital theoretical predictions that underscore the phase-sensitive potential of beam shifts, the direct experimental realization of utilizing beam-shift spectroscopy to resolve fine electronic structures in moiré materials remains unachieved. Their application to twist-angle-dependent electronic states remains unexplored. The unique advantage of the GH shift lies in its intrinsic connection to interfacial optical responses, making it particularly amenable to twist-angle control in TBG. Most significantly, because the GH shift directly measures the phase gradient of reflected light, it can circumvent the resolution limits of conventional optical techniques, thereby enabling the first experimental observation of electron–hole asymmetry in large-twist-angle TBG.

In this paper, we demonstrate that the GH shift spectra in TBG can be precisely controlled through VHSs energy tuning at different twist angles. Crucially, we present the first experimental observation of split spectral features in the GH shift profiles, which correspond to $\tilde{n}$ splitting at VHSs resonances—a phenomenon predicted by tight-binding (TB) models for twist angles $\theta > 10°$ due to the electron–hole asymmetry [7,14–16]. Our measurements indicate that the splitting interval remains below 100 meV for twist angles between 10° and 15°, with its magnitude exhibiting a clear dependence on the interlayer coupling strength and interlayer distance. These findings establish GH shift spectroscopy as a powerful new tool for characterizing moiré superlattices, while opening avenues for investigating band structure topologies, optoelectronic properties, and interlayer interactions in twisted heterostructures [32].

2. MATERIALS AND METHODS

A. Sample Fabrication Methods

Single-layer graphene (SLG) and few-layer hexagonal boron nitride (h-BN) are fabricated by mechanical exfoliation. Using a high-precision rotational stage, SLG is cleaved, rotated, and restacked to form TBG (see also Supplement 1, Section 1 and Refs. [6,33] therein). Prepare a 0.8 mg/10 ml polycarbonate (PC) solution in chloroform. Spin-coat the PC solution onto a clean silicon substrate to form a uniform PC film, then transfer it onto polydimethylsiloxane (PDMS). On a stacking transfer platform, adhere the PDMS/PC structure to thin h-BN, followed by heating. After cooling and lifting the structure, the h-BN will adhere to the PC layer. Place the h-BN sheet on one half of a large-size SLG. Lift the assembly to tear out an SLG with the same crystal orientation. Rotate the remaining SLG on the substrate by a desired angle using a rotation stage. Align and adhere the SLG attached to h-BN with the rotated SLG on the substrate, forming TBG via interlayer van der Waals forces. Lift the assembly, leaving the TBG attached to the h-BN sheet. Place the h-BN/PC/PDMS structure with the attached TBG onto a K9 glass substrate. Heat the structure to separate the PDMS from the PC film. Remove the PDMS layer, leaving the PC-covered and h-BN-encapsulated TBG sample on the K9 glass substrate. Dissolve the PC film on the sample surface using chloroform. The preparation method for AB-stacked bilayer graphene (AB-BLG) with h-BN is similar to that for TBG: h-BN is used to transfer mechanically exfoliated bilayer graphene onto a K9 substrate, followed by cleaning the PC with chloroform.

B. Sample Characterization

Optical images were captured using WITec Alpha 300RAS by a 100× objective lens (Zeiss EC Epiplan-Neofluar Dic 100×/0.9). Transmission absorption spectra were performed on WITec Alpha 300RAS with a halogen tungsten lamp (Thorlabs SLS201L/M) and focused by an objective lens (Nikon 50×/0.6). Then collect the transmitted light intensity signal through an objective lens (Zeiss EC Epiplan-Neofluar Dic 100×/0.9). Raman spectroscopy was performed on a confocal Raman spectrometer (WITec Alpha 300RAS). A continuous-wave (CW) laser with a wavelength of 532 nm (laser power is 2 mW) was focused by a 100× objective lens (Zeiss EC Epiplan-Neofluar Dic 100×/0.9) as excitation light. Atomic force microscopy (AFM) of h-BN on samples was performed using a WITec Alpha 300RAS system equipped with contact-mode AFM sensors (spring constant $k = 0.2$ N/m; resonant frequency $f = 14$ kHz).

C. GH Shift Spectra Characterization

The laser beam was generated by a supercontinuum laser (NKT Photonics, WL-SC-400-15). A radio-frequency (RF) driver (NKT Photonics, External RF Driver) drives an acousto-optic modulator. The acousto-optic modulator (AOM) (NKT Photonics, SuperK SELECT) filters and outputs a single-wavelength beam. A Glan–Taylor prism (Thorlabs, GL15) was used to generate the linearly polarized incident light. The half-wave plate (HWP) (Thorlabs, AHWP10M-600) was used to change the polarization state of the light. O1 is a 20× long-working distance objective lens (Nikon, TU Plan ELWD) and is used to focus the laser on the sample. An infinity-corrected microscope magnification system, comprising O2 (OptoSigma, PAL-50-L-A) and a tube lens ($f = 400$ mm), was used to collect the reflected light and amplify the beam displacement. A position-sensitive detector (PSD) (HAMAMATSU, S3931) positioned at the focal plane was used to determine the position of the beam. The position data were collected by an oscilloscope (Tektronix, MSO2024B). The prism used in the experiment was made of K9 glass and purchased from Daheng Optics, China. The substrate and the prism were attached by the index-matching fluid to ensure that they were a uniform medium. We used cedar wood oil ($n = 1.51$) as the refractive index matching fluid to ensure that the substrate was loosely mounted so that stress-induced birefringence could be avoided.

3. RESULTS AND DISCUSSION

A. VHSs and Transmission Absorption Spectra in TBG

The relative twist angle between the two graphene layers produces a moiré superlattice, which modifies the electronic band structure, as shown in Fig. S5 in Section 3 of Supplement 1. Saddle points in the band structure led to a pronounced enhancement of the density of states (DOS) at specific energies, giving rise to VHSs. As shown in Fig. 1(a), the separation between the two Dirac cones varies with the twist angle, thereby modulating the binding energy of VHSs. The presence of VHSs significantly enhances the optical transition probability, yielding distinct absorption peaks in the spectra. The evolution of these VHSs with the twist

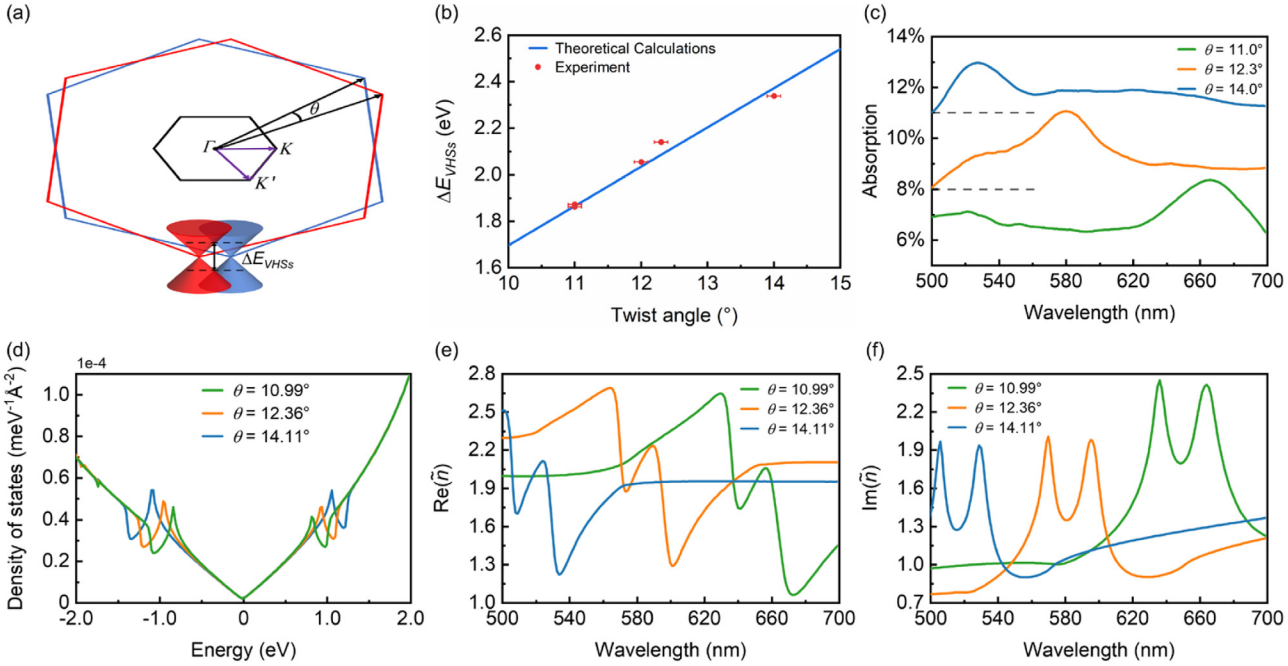

Fig. 1. Twist-angle-dependent VHSs in TBG. (a) Illustration of the relationship between the energy of the VHSs and the twist angle θ in TBG. As the twist angle θ increases, the increased separation between the Dirac cones of the two layers leads to a larger energy separation between the VHSs. (b) The energy of the VHSs for different twist angles (see detailed discussions in Supplement 1, Section 2.A and Ref. [5]), with the best fitted Fermi velocity of 0.87×10^6 m/s, with data points corresponding to the absorption peak energies measured from TBG with twist angles of 11.0°, 12.0°, 12.3°, and 14.0°. (c) Smoothed experimental transmission absorption spectra for TBG with different twist angles (dashed lines). Spectra are offset in absorption by 3% apiece for clarity. (d)–(f) Calculation results of TBG with different twist angles using the TB model: (d) DOS, (e) Re($\tilde{n}$), and (f) Im($\tilde{n}$).

angle leads to systematic shifts in the absorption peaks, as shown in Figs. 1(b) and 1(c), with the absorption peaks observed at 665.47 ± 0.29 nm, 579.34 ± 0.37 nm, and 530.12 ± 0.48 nm for the 11.0°, 12.3°, and 14.0° TBG (Supplement 1, Section 2.A), respectively. A comparison between the experimental data points and the absorption peak energies in Fig. 1(b) reveals that the twist angle of the fabricated TBG sample closely matches the rotation angle targeted by the stacking apparatus.

B. TB Model in TBG

For TBG, the TB model can be used to calculate the band structures and the complex refractive index. Using the p_z-orbital TB model, we calculated the eigenenergies and eigenfunctions of TBG, with the Hamiltonian written as [14,15]

$$H = \sum_i V_i \left|R_i\right\rangle \left\langle R_j\right| - \sum_{\langle i,j\rangle} t\left(R_i - R_j\right) \left|R_j\right\rangle \left\langle R_i\right| + \text{h.c.}, \tag{1}$$

where $|R_i\rangle$ denotes the atomic p_z state at lattice site $\vec{R}_i$, V_i is the on-site energy, and $t(\vec{R}_i - \vec{R}_j)$ is the transfer integral between sites i and j. For pristine graphene, we take the Dirac point as the energy reference and set $V_i = 0$. The second sum runs over ordered nearest-neighbor pairs, and h.c. denotes the Hermitian conjugate $t^*(\vec{R}_i - \vec{R}_j)|R_i\rangle\langle R_j|$, ensuring that the Hamiltonian is Hermitian. The transfer integral is parametrized by the Slater–Koster formulas given in Eq. (2). We can approximate it as

$$-t(\vec{d}) = V_{pp\pi}\left[1 - \left(\frac{\vec{d}\cdot\vec{e}_z}{d}\right)^2\right] + V_{pp\sigma}\left(\frac{\vec{d}\cdot\vec{e}_z}{d}\right)^2, \tag{2}$$

$$V_{pp\pi} = V^0_{pp\pi} \exp\left(-\frac{d-a_0}{\delta_0}\right), \tag{3}$$

$$V_{pp\sigma} = V^0_{pp\sigma} \exp\left(-\frac{d-d_0}{\delta_0}\right), \tag{4}$$

where $a_0 \approx 0.142$ nm and $d_0 = 0.335$ nm are the carbon–carbon distance and the interlayer distance of TBG, respectively. $V^0_{pp\pi}$ and $V^0_{pp\sigma} = 480$ meV are the intralayer and interlayer hopping integrals, respectively. $\delta_0 = 0.184\sqrt{3}a_0$ is the decay length of the hopping integral. To obtain approximately the same Fermi velocity from the TB model, the intralayer hopping is set to be $V^0_{pp\pi} = 3200$ meV. For the twist angle of 11.0°, we find a commensurate angle close to it based on the geometric relations with the parameter $(m_0, r) = (5, 2)$ [34].

By using the TB model, $\tilde{n}$ of TBG with different twist angles was obtained. It was observed that Im($\tilde{n}$) exhibits peaks at the VHSs, which shift toward higher energies as the TBG twist angle increases—a trend that perfectly echoes the blueshift of the experimental absorption peaks with increasing twist angle [Figs. 1(c), 1(e), and 1(f)]. This indicates that TBG has the potential to modulate the GH shift spectra by altering the interlayer twist angle to adjust the complex refractive index.

In contrast to the double-peak (valley) structure evident in $\tilde{n}$ [Figs. 1(e) and 1(f)]—arising from electron–hole asymmetry in TB model calculations for large-twist-angle TBG [14,15]—only a single peak is discernible in the absorption spectrum due to optical broadening. This constraint impedes further optical exploration of the electronic and optical properties of large-twist-angle TBG.

C. GH Shift Spectroscopy and the Multilayer Film Reflection Model

The experimental setup of the GH shift spectroscopy is shown in Fig. S6 in Section 4 of Supplement 1. The supercontinuum spectral

light source emits laser light, which is modulated by an AOM via an RF driver to select different wavelengths. The polarization of the incident light is adjusted using a HWP to switch between s- or p-polarization. The position of the prism is adjusted to focus the light beam on the sample surface, which is then confirmed using a charge-coupled device (CCD) camera. The reflection beam's position is measured directly using the beam displacement amplification technique (BDAT) and a PSD. By using a program to automatically adjust the wavelength of the incident light and collect the position data, we can obtain the GH shift spectra of different optical interfaces. However, achieving control over the GH shift remains a major challenge.

The GH shift originates from the dispersion of the transmitted and reflected beams, where the incident light is composed of plane waves of different angular spectra. To calculate the GH shift numerically, we need the reflection coefficients $r^{s,p}$ for s- and p-polarized light. Here, we employ a multilayer thin-film reflection model and the transfer matrix method to perform the calculation [19,22,35]:

$$r^{s,p} = \frac{E_{01}^{+}}{E_{01}^{-}} = \frac{r_{01}^{s,p} + r_{12}^{s,p} e^{2i\delta_1}}{1 + r_{01}^{s,p} r_{12}^{s,p} e^{2i\delta_1}}, \tag{5}$$

where $\delta_1 = \frac{2\pi}{\lambda}\tilde{n}_1 h_1 \cos\theta_1$ is the phase factor, $\tilde{n}_1 = n + ik$ is the complex refractive index of the 2D material, h_1 is the thickness of the 2D material, and θ_1 is the incident angle. $r_{jk}^{s,p} = |r^{s,p}|e^{i\varphi^{s,p}}$ represents the complex Fresnel reflection coefficient of s- or p-polarized light at the j–k interface (see details in Supplement 1, Section 4.A). The GH shift can be calculated from the Fresnel coefficients [19,22,35]:

$$\Delta_{\mathrm{GH}} = -\frac{1}{k_0}\left(w^s \frac{\partial\varphi^s}{\partial\theta_0} + w^p \frac{\partial\varphi^p}{\partial\theta_0}\right), \tag{6}$$

where $k_0 = \frac{2\pi n_0}{\lambda}$, $w^{s,p} = \frac{(a^{s,p}|r^{s,p}|)^2}{(a^s|r^s|^2)+(a^p|r^p|^2)}$, and $a^{s,p}$ are the electric field components. When $a^s = 1$, $\Delta_{\mathrm{GH}} = \Delta_s$. Similarly, when $a^p = 1$, $\Delta_{\mathrm{GH}} = \Delta_p$. The GH shift is often investigated using $\Delta_s - \Delta_p$. From Eq. (6), we can know that the responses in the GH shift spectra are directly relevant to the optical properties of the materials since $\tilde{n}$ of the materials participates in the Fresnel coefficients. Therefore, the GH shift can be controlled by adjusting $\tilde{n}$.

D. Tunable GH Shift Spectra in TBG

Based on the TB model, we scanned the GH shift spectra with a 45° incident angle over different twist angles and showed the theoretically feasible adjustments of the GH shift spectra [Figs. 2(b) and 2(c)]. These results explicitly manifest the efficient control of the GH shift through handling the interlayer twist angle in TBG. Using the fabricated TBG (Fig. S2 in Section 2 of Supplement 1), we obtained the experimental GH shift spectra results with a 45° incident angle shown in Figs. 2(d)–2(f) and Fig. S10 of Supplement 1. The GH shift spectra show unique split characteristics absent from the absorption spectra of 11.0°, 12.0°, 12.3°, and 14.0° TBG, which closely follow the variation trend of $\tilde{n}$ in the spectra calculated by the TB model.

For 11.0° TBG [Fig. 2(d)], the GH shift valley is split into two at 641.78 ± 2.80 nm and 665.52 ± 1.70 nm, with an energy separation of 68.92 ± 9.67 meV. For 12.0° TBG [Fig. S10(b) in Section 4 of Supplement 1], the GH shift valley is split at 589.83 ± 1.49 nm and 610.28 ± 1.28 nm, with an energy separation of 70.45 ± 6.81 meV. For 12.3° TBG [Fig. 2(e)], the GH shift valley is split at 561.39 ± 1.30 nm and 586.48 ± 1.38 nm, with an energy separation of 94.49 ± 7.14 meV. For 14.0° TBG [Fig. 2(f)], the GH shift valley is split at 512.29 ± 1.10 nm and 526.67 ± 2.74 nm, with an energy separation of 66.10 ± 13.29 meV. We also fabricated an additional 11.0° sample [Fig. S7(e) in Section 4 of Supplement 1]. We discovered that the GH shift valley is split at 629.68 ± 0.52 nm and 653.13 ± 1.24 nm, with an energy separation of 70.69 ± 3.97 meV. Detailed experimental data are available in Fig. S10 and Tables S3–S5 in Section 4 of Supplement 1. As shown in Fig. 2(g), the two valley positions in the GH shift spectra undergo a blueshift as the twist angle increases, demonstrating consistency with the experimental results in Figs. 1(b) and 1(c) and the simulated results in Figs. 2(b) and 2(c). Consequently, despite the emergence of a distinctive double-valley profile in the GH shift spectra of TBG at large twist angles, the robust twist-controlled tunability of the valley wavelength (energy) remains entirely achievable. By extracting the differences in both wavelength and energy between the two valleys [Figs. 2(h) and 2(i)], we find that the splitting magnitude is strictly bounded below 30 nm (100 meV). Such a subtle splitting is naturally obscured and challenging to discern via conventional optical characterizations, such as traditional absorption spectroscopy. These results highlight the great promise of GH shift spectroscopy implemented via BDAT for resolving the fine structures of 2D materials at the microscale.

To eliminate potential interference from the h-BN encapsulation, we conducted comparative measurements of the GH shift spectra between h-BN-covered AB-stacked bilayer graphene and bare AB-stacked bilayer graphene [Fig. S11(a) in Section 4 of Supplement 1]. The results show that while the h-BN-covered sample maintains a linear GH shift spectrum, it only exhibits minor shifts relative to the uncovered sample [Fig. S11(b) in Section 4 of Supplement 1]. This confirms that the appearance of the valleys in the GH shift spectra of TBG is unrelated to the presence of h-BN. Additionally, we simulated the GH shift spectra of TBG encapsulated by h-BN with various thicknesses, as shown in Fig. S8 in Section 4 of Supplement 1. Utilizing the TB model, calculations for the 10.99° TBG combined with different h-BN thicknesses reveal that the presence of h-BN merely induces an overall rigid shift in the magnitude of the GH shift, leaving the spectral positions of the valleys practically unaltered. Since our experimental analysis primarily concerns the spectral information encoded in the wavelength (energy) domain, the simulated GH shift spectra presented throughout this work exclude the effect of h-BN. This rigid offset does not affect the extraction of valley positions or splitting energies.

E. Electron–Hole Asymmetry in TBG

As shown in Figs. 1(e) and 1(f), the calculation results of $\mathrm{Re}(\tilde{n})$ and $\mathrm{Im}(\tilde{n})$ are split into two. However, for the absorption spectra, only one broad peak can be captured. Using the TB model, we calculated the band structure and $\mathrm{Im}(\tilde{n})$ for 10.99° TBG, with the results shown in Figs. 3(a) and 3(b). In Fig. 3(b), the two $\mathrm{Im}(\tilde{n})$ peaks for 10.99° TBG are located at 632.78 and 666.22 nm, with an energy separation of 98.38 meV.

By calculating the resonance distributions of the $\mathrm{Im}(\tilde{n})$ peaks over the moiré Brillouin zone, we found that the two $\mathrm{Im}(\tilde{n})$ peaks correspond to resonances occurring near and around the Γ point

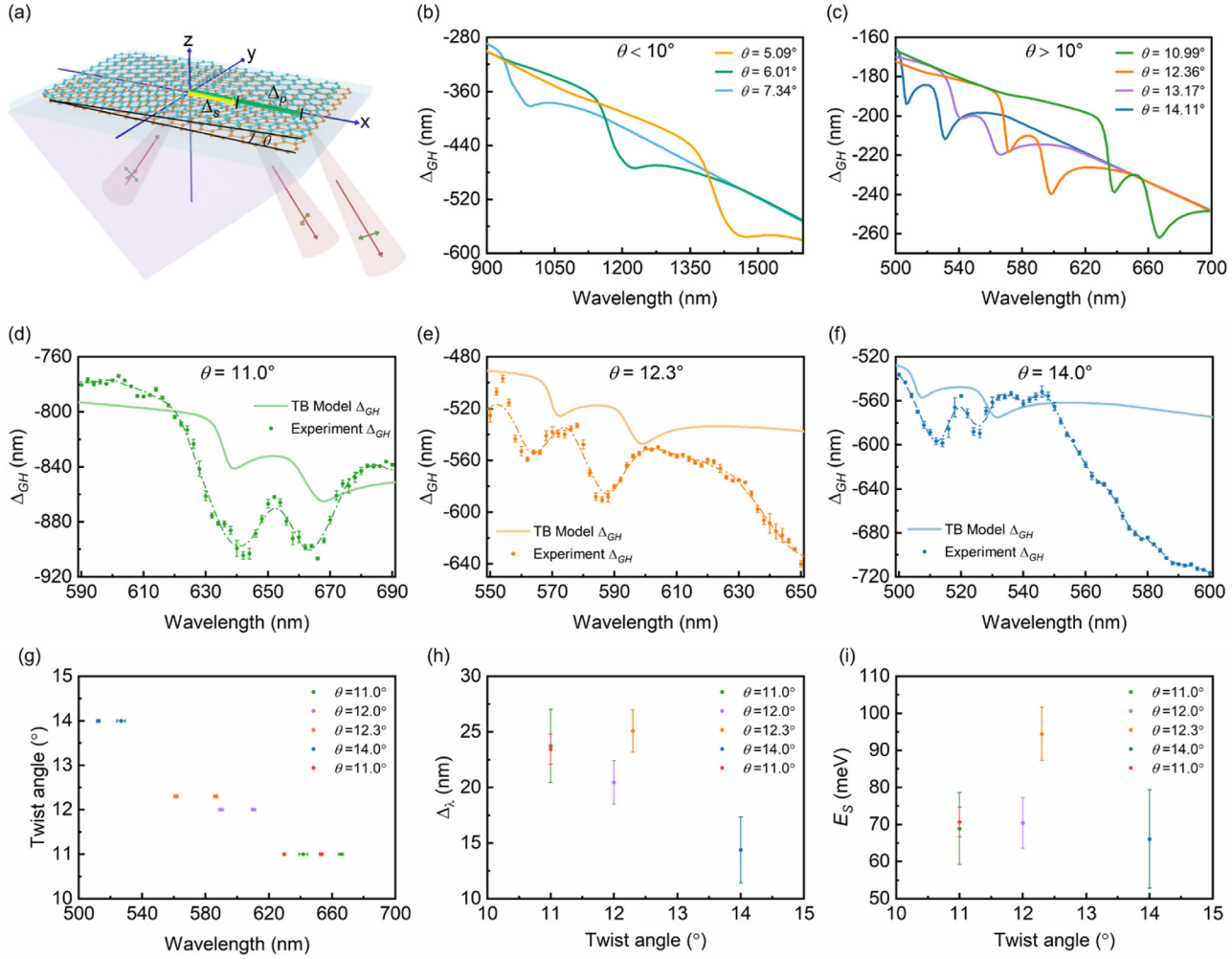

Fig. 2. Tunable GH shift spectra in TBG. (a) Schematic diagram of the GH shift ($\Delta_{s,p}$) originating from the s-polarized light (yellow) and p-polarized light (green) for TBG with the twist angle θ. (b) TB model results of GH shift spectra for the twist angle $\theta < 10°$. (c) TB model results of GH shift spectra for the twist angle $\theta > 10°$. Experimental results (symbols with error bars, with the dashed-dotted lines representing the corresponding smoothed data) and TB model calculations (light-colored curves) of GH shift spectra for (d) 11.0°, (e) 12.3°, and (f) 14.0° TBG. The commensurate angles we take for the TB model are 10.99°, 12.36°, and 14.11°. Due to the encapsulation of the TBG samples in h-BN, the experimental results of the GH shift will be shifted as a whole (see Supplement 1, Sections 4.A and 4.C). Note that the simulated GH shift results exclude the influence of h-BN, and the axes have been adjusted to match the range of the experimental data. (g) Peak wavelengths of the two valleys extracted via Lorentzian fitting from the GH shift spectra of TBG at various twist angles. (h) Wavelength separation (Δ_λ) and (i) energy splitting (E_S) between the two valleys in the GH shift spectra of TBG with different twist angles.

in the moiré Brillouin zone, respectively. Through verification (Supplement 1, Section 5), the resonances originate from the transition processes labeled by blue and red arrows in the band structure in Fig. 3(a). From the perspective of the spectra, when the energy of the incident light is relatively small, it is mainly the electrons around the Dirac cone that are excited, forming two resonance rings around K and K′ points in the moiré Brillouin zone [Fig. 3(d)]. These transition processes only result in constant absorption in the low-energy range, which can be deemed as two independent sheets of graphene.

When the incident photon energy increases, the optical transitions involve further bands in the high-energy range and experience enhanced resonances by touching the VHSs [Figs. 3(e) and 3(f)], which exhibit electron–hole asymmetry that is especially pronounced for $\theta > 10°$ situations [7,14–16]. This explains the splitting of the interband-excitations-induced valleys. Due to optical broadening, this tiny splitting is difficult to observe directly in the absorption spectra (for a detailed discussion about broadening, see Supplement 1, Section 4.E).

The split energy of the theoretical calculations is around 100 meV, which is larger than the values observed experimentally. This quantitative difference reflects the effective interlayer coupling realized in the measured samples. In the Slater–Koster parametrization of Eq. (2), both the bare amplitude $V^0_{pp\sigma}$ and the interlayer distance d_0 control the same effective interlayer hopping: changing $V^0_{pp\sigma}$ scales the coupling linearly, whereas changing d_0 modifies it exponentially. They are therefore not independent fitting parameters but two ways of tuning a single effective coupling strength. Figure 3(c) shows how the splitting energy varies with $V^0_{pp\sigma}$ for the measured twist angles; the experimental splittings are reproduced when the effective coupling is somewhat smaller than 480 meV. A single unified value is difficult to justify, because the actual interlayer distance of each fabricated sample is not measured and may vary with the stacking conditions. This interpretation

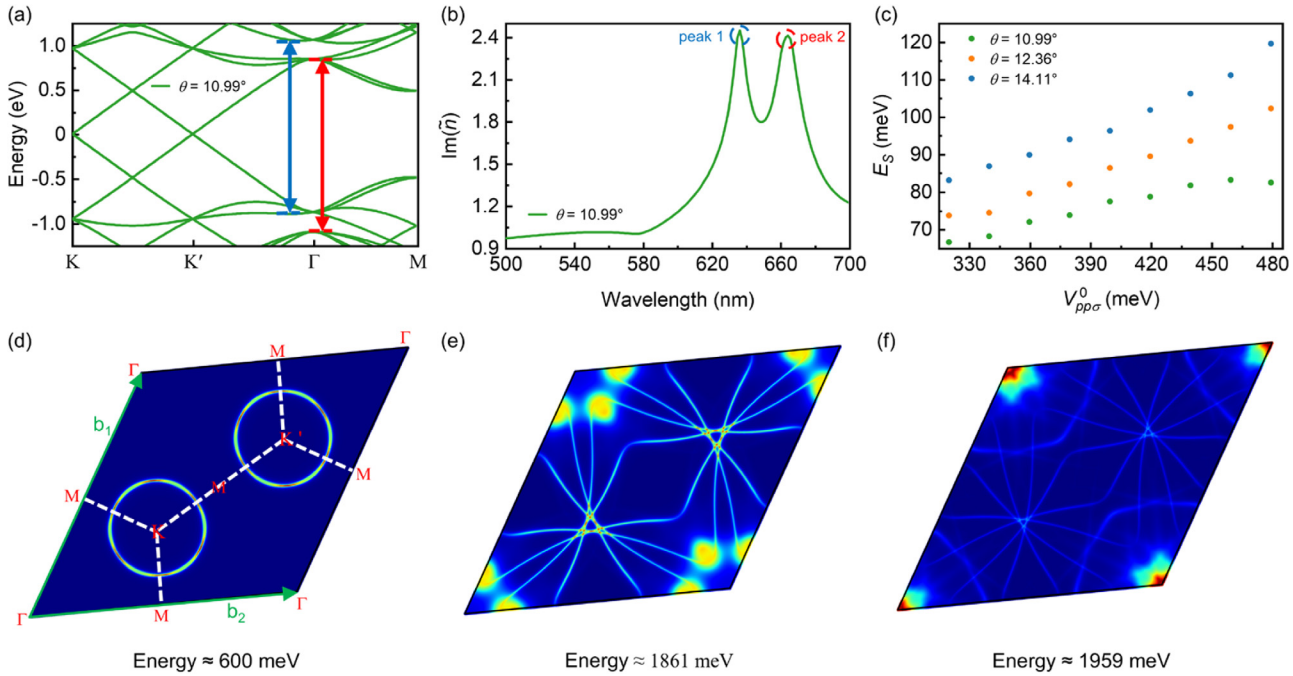

Fig. 3. Calculation results for electron–hole asymmetry in TBG. (a) The band structure of 10.99° TBG, where the blue and red arrows label two kinds of transitions corresponding to the resonance peaks 1 and 2 in (b). (b) Calculation of Im($\tilde{n}$) for 10.99° TBG. Peaks 1 and 2, which originate from the transitions in (a), are situated around 633 and 666 nm, respectively, with an energy separation of 98.38 meV. (c) Relationship between the splitting energy and the interlayer coupling for different twist angles. Calculated resonance distribution over the moiré Brillouin zone for (d) $E \approx 600$ meV, (e) $E \approx 1861$ meV, and (f) $E \approx 1959$ meV (b_1 and b_2 are the reciprocal lattice vectors of the moiré Brillouin zone).

is consistent with the two 11.0° samples, which yield splittings of 68.92 ± 9.67 meV and 70.69 ± 3.97 meV and therefore require slightly different effective couplings. We thus attribute the remaining quantitative discrepancy to a sample-dependent renormalization of the effective interlayer coupling, not to a breakdown of the model. We calculated the variations of the split energy over different interlayer coupling $V^0_{pp\sigma}$ and found that the split energy changes with decreasing $V^0_{pp\sigma}$ [Fig. 3(c)]. Meanwhile, the interlayer distance between two graphene layers will also influence the coupling strength according to the exponential relations in Eq. (2) and Fig. S12 in Section 4 of Supplement 1. This implies that the coupling parameter $V^0_{pp\sigma}$, in combination with the interlayer spacing employed in the TB model calculations, jointly results in overestimations of the valley split within the actual experimental samples.

4. CONCLUSION

In summary, we have experimentally validated the correspondence between GH shift spectra and optical absorption measurements, demonstrating the precise control of GH shift signatures through interlayer twist angle modulation in TBG. The observed valleys in the GH shift spectra arise from enhanced resonances at VHSs, which are systematically tuned into low-energy regimes via twist engineering. Notably, we report the first experimental observation of split GH valleys in TBG optical measurements, which can be theoretically attributed to electron–hole asymmetry, particularly prominent at larger twist angles. Although this occurs in a higher-energy regime than the magic-angle phenomena, both originate from the same interlayer coupling mechanisms. Our findings therefore provide complementary insight into twist-controlled electronic asymmetry and offer a new phase-sensitive probe that bridges optical and electronic perspectives of TBG physics. Such splitting, typically below 100 meV and obscured by optical broadening in conventional absorption spectroscopy, demonstrates the superior sensitivity of GH shift measurements. By using the splitting energy obtained from the GH shift spectra, we can constrain key parameters like the interlayer coupling strength in the TB model, making the simulations more representative of real experimental conditions. This distinction underscores the complementary value of GH shift spectra in probing subtle electronic interactions that conventional optical methods may overlook.

Since the establishment of the optical shift spectra, current results have proven their outperformance over other traditional optical spectra methods such as optical absorption or photoluminescence, etc. Accurate characterizations of optical properties, such as the ground excitons in the monolayer WS_2 [26], the Rydberg excitons in the monolayer MoS_2 [36], and now the split features of TBG, have highlighted the enormous potential of the optical shift spectra. These advancements could significantly impact applications in precise measurement, biological sensing, and probing quantum systems, among others. On the other hand, the twist angle of TBG can play a direct and convenient handle in controlling the GH signatures. In the future, this method could facilitate a deeper understanding of complex physical phenomena in 2D and nanoscale materials, such as band structures, intra- and interlayer excitons, self-trapped excitonic effects, material anisotropy, and interlayer interactions.

Funding. National Natural Science Foundation of China (12574339, 12574457, 12174207, 12374273, 12421005, 11935006, 12247105); Tianjin Science and Technology Project (24ZXZSSS00120); Hunan Provincial Major Sci-Tech Program (2023ZJ1010); National Key R&D Program (2024YFE0102400);

Quantum Science and Technology-National Science and Technology Major Project (2024ZD0301000).

Acknowledgment. J. X. Tu prepared the samples of TBG and h-BN-covered bilayer graphene; J. X. Tu performed the transmission absorption spectra, Raman spectroscopy, atomic force microscopy (AFM), and GH shift spectra measurements; X. F. Li. performed the TB model calculations; and J. X. Tu, X. F. Li, and Y. P. Yan analyzed the data. The paper was written by J. X. Tu and X. F. Li with contributions from Y. P. Yan, X. Li, X. X. Zhou, H. Jing, L. M. Kuang, X. F. Chen, J. G. Tian, and Z. B. Liu. X. Li, X. X. Zhou, and Z. B. Liu supervised the project.

Disclosures. The authors declare no conflicts of interest.

Data availability. All of the data that support the findings of this study are reported in the main text and the supplemental document. Source data are available from the corresponding author upon reasonable request. Correspondence and requests for materials should be addressed to X. Li, X. X. Zhou, and Z. B. Liu.

Supplemental document. See Supplement 1 for supporting content.

REFERENCES

1. Y. Cao, V. Fatemi, S. Fang, *et al.*, "Unconventional superconductivity in magic-angle graphene superlattices," Nature **556**, 43–50 (2018).
2. R. Bistritzer and A. H. MacDonald, "Moiré bands in twisted double-layer graphene," Proc. Natl. Acad. Sci. USA **108**, 12233–12237 (2011).
3. E. Y. Andrei, D. K. Efetov, P. Jarillo-Herrero, *et al.*, "The marvels of moiré materials," Nat. Rev. Mater. **6**, 201–206 (2021).
4. G. Trambly de Laissardière, D. Mayou, and L. Magaud, "Localization of Dirac electrons in rotated graphene bilayers," Nano Lett. **10**, 804–808 (2010).
5. A. K. Geim and I. V. Grigorieva, "Van der Waals heterostructures," Nature **499**, 419–425 (2013).
6. H. Peng, N. B. Schröter, J. Yin, *et al.*, "Substrate doping effect and unusually large angle van Hove singularity evolution in twisted bi-and multilayer graphene," Adv. Mater. **29**, 1606741 (2017).
7. R. W. Havener, Y. Liang, L. Brown, *et al.*, "Van Hove singularities and excitonic effects in the optical conductivity of twisted bilayer graphene," Nano Lett. **14**, 3353–3357 (2014).
8. J. L. dos Santos, N. Peres, and A. C. Neto, "Graphene bilayer with a twist: electronic structure," Phys. Rev. Lett. **99**, 256802 (2007).
9. H. Ribeiro, K. Sato, G. Eliel, *et al.*, "Origin of van Hove singularities in twisted bilayer graphene," Carbon **90**, 138–145 (2015).
10. Y. Wang, Z. Ni, L. Liu, *et al.*, "Stacking-dependent optical conductivity of bilayer graphene," ACS Nano **4**, 4074–4080 (2010).
11. Y. Cao, D. Rodan-Legrain, O. Rubies-Bigorda, *et al.*, "Tunable correlated states and spin-polarized phases in twisted bilayer–bilayer graphene," Nature **583**, 215–220 (2020).
12. X. Lu, P. Stepanov, W. Yang, *et al.*, "Superconductors, orbital magnets and correlated states in magic-angle bilayer graphene," Nature **574**, 653–657 (2019).
13. Y. Cao, V. Fatemi, A. Demir, *et al.*, "Correlated insulator behaviour at half-filling in magic-angle graphene superlattices," Nature **556**, 80–84 (2018).
14. P. Moon and M. Koshino, "Optical absorption in twisted bilayer graphene," Phys. Rev. B **87**, 205404 (2013).
15. P. Moon, Y.-W. Son, and M. Koshino, "Optical absorption of twisted bilayer graphene with interlayer potential asymmetry," Phys. Rev. B **90**, 155427 (2014).
16. A. Vela, M. Moutinho, F. Culchac, *et al.*, "Electronic structure and optical properties of twisted multilayer graphene," Phys. Rev. B **98**, 155135 (2018).
17. D. Basov, M. Fogler, and F. García de Abajo, "Polaritons in van der Waals materials," Science **354**, aag1992 (2016).
18. F. Goos and H. Hänchen, "Ein neuer und fundamentaler Versuch zur Totalreflexion," Ann. Phys. **436**, 333–346 (1947).
19. K. Artmann, "Berechnung der Seitenversetzung des totalreflektierten Strahles," Ann. Phys. **437**, 87–102 (1948).
20. D.-K. Li, S.-Y. Wang, X.-Q. Yan, *et al.*, "Anisotropic Goos–Hänchen shift in few-layer two-dimensional materials," Appl. Phys. Lett. **120**, 053105 (2022).
21. X. Qiu, X. Zhou, D. Hu, *et al.*, "Determination of magneto-optical constant of Fe films with weak measurements," Appl. Phys. Lett. **105**, 131111 (2014).
22. N. Hermosa, "Reflection beamshifts of visible light due to graphene," J. Opt. **18**, 025612 (2016).
23. D. Li, B. Su, R. Wen, *et al.*, "Abnormal spatial shifts in graphene measured via the beam displacement amplification technique: implications for sensors based on the Goos–Hänchen effect," ACS Appl. Nano Mater. **4**, 13477–13485 (2021).
24. N. Mao, J. Tang, L. Xie, *et al.*, "Optical anisotropy of black phosphorus in the visible regime," J. Am. Chem. Soc. **138**, 300–305 (2016).
25. L.-G. Wang, H. Chen, and S.-Y. Zhu, "Large negative Goos–Hänchen shift from a weakly absorbing dielectric slab," Opt. Lett. **30**, 2936–2938 (2005).
26. M. Zha, X. Li, E. Xu, *et al.*, "Optical shift spectroscopy in two-dimensional materials," Optica **11**, 344–353 (2024).
27. X. Zhou, X. Ling, H. Luo, *et al.*, "Identifying graphene layers via spin Hall effect of light," Appl. Phys. Lett. **101**, 251602 (2012).
28. M. J. Park, Y. Kim, G. Y. Cho, *et al.*, "Higher-order topological insulator in twisted bilayer graphene," Phys. Rev. Lett. **123**, 216803 (2019).
29. W. J. de M. Kort-Kamp, "Topological phase transitions in the photonic spin Hall effect," Phys. Rev. Lett. **119**, 147401 (2017).
30. W. J. M. Kort-Kamp, F. J. Culchac, R. B. Capaz, *et al.*, "Photonic spin Hall effect in bilayer graphene moiré superlattices," Phys. Rev. B **98**, 195431 (2018).
31. Z. Chen, H. Yang, Y. Xiao, *et al.*, "Photonic spin Hall effect in twisted bilayer graphene," J. Opt. Soc. Am. A **38**, 1232–1236 (2021).
32. A. Aiello and J. Woerdman, "Role of beam propagation in Goos–Hänchen and Imbert–Fedorov shifts," Opt. Lett. **33**, 1437–1439 (2008).
33. J. L. dos Santos, N. Peres, and A. C. Neto, "Continuum model of the twisted graphene bilayer," Phys. Rev. B **86**, 155449 (2012).
34. A. Sboychakov, A. Rakhmanov, A. Rozhkov, *et al.*, "Electronic spectrum of twisted bilayer graphene," Phys. Rev. B **92**, 075402 (2015).
35. S. Grosche, M. Ornigotti, and A. Szameit, "Goos-Hänchen and Imbert-Fedorov shifts for Gaussian beams impinging on graphene-coated surfaces," Opt. Express **23**, 30195–30203 (2015).
36. X. Li, J. Tu, Z. Du, *et al.*, "Observation of Rydberg excitons in monolayer MoS_2 at room temperature by Imbert-Fedorov shift spectroscopy," Phys. Rev. B **110**, 235413 (2024).